Infrastructure-User Heterogeneous Data Interaction and Fusion of Mobile-IoT Sensing Networks in a Smart City: Application to a Footbridge

Yixian Li, Qi Xia, Tong Guo, Yuxuan Zhang, Wanglin Wu, and Yong Xia

***Abstract*—Abundant data are collected in the daily operation of infrastructures via structural health monitoring (SHM) systems. Meanwhile, user information is measured through the popularized mobile smartphones nowadays. However, these data types are insufficiently integrated or fused to extract valuable information to improve user comfort or enhance infrastructure safety. In this study, a bidirectional data interaction framework is developed to facilitate information sharing and fusion among users and the infrastructure through wired and wireless communications. The framework is applied to an overpass footbridge equipped with an SHM system. The walking patterns and dynamic information of pedestrians are extracted from the acceleration, orientation, and GPS data of smartphones. On this basis, the pedestrian load is generated and applied to the numerical model of the footbridge, and the full-field bridge responses can be calculated to realize a virtual holographic sensing. Simultaneously, the micro-environment and vibration data of the footbridge are collected from the SHM system, smartphones, and online databases. These data are formulated as the pedestrian comfort indexes, which directly determine the behavior and perception of pedestrians to their surroundings. The in-field data in a week are used to verify the applicability and performance of the developed approach. Results show that the data integration framework can improve the volume and diversity of data for infrastructures and users with satisfactory accuracy.**

***Index Terms*—Mobile Sensing, IoT Network, Heterogeneous Data Integration, User-Infrastructure Interaction, SHM, Micro Environment Comfort.**

I. INTRODUCTION

MODERN cities face increasing risks due to large populations and crowded construction. Numerous sensors are consequently installed to measure different types of information in urban areas, such as weather stations, cameras, and smoke and fire alarms [1-3]. In recent decades, structural health monitoring (SHM) technologies have been developed to evaluate the safety and risk of infrastructures [4]. Recent advancements in sensors [5], big data [6], edge computing [7], and artificial intelligence [8, 9] have enhanced the performance and applicability of SHM.

An SHM system is composed of distributed sensors, such as thermometers, weather stations, cameras, accelerometers, strain gauges, and GPS [10, 11], from which the environmental effects, external loads, and structural responses are measured. Sensors are installed at fixed locations, and the measurable information is therefore limited [12, 13]. However, abundant high-cost sensors are required to collect sufficient data on large-size infrastructures [14, 15].

With the rapid popularization of smartphones worldwide, the Internet of Things (IoT)-supported smart city becomes a feasible future via mobile crowdsensing systems [1, 16]. The GPS, accelerometer, gyroscope, microphone, magnetometer, and light meter [17] are embedded in smartphones. They can supplement the sensor network in the existing SHM systems due to the ubiquity of smartphones; these mobile sensors can even be organized as an independent wireless sensor network [18]. At the same time, smartphone-sensing-aided SHM faces challenges, such as the huge amount of data traffic, low data accuracy, and inadequate number of participants [19]. Recent advances and applications of smartphone-aided SHM are reviewed as follows.

The embedded accelerometers of smartphones can measure the vibration of infrastructures, from which natural frequencies and mode shapes of a structure can be identified. In the early days, Feng et al. [20] conducted a shaking table experiment on a masonry column to examine the accuracy of smartphone acceleration data. The natural frequencies of a laboratory steel frame were successfully identified by Ozer et al. [21] using the acceleration and gyroscope data, where the orientation of the smartphone was determined using the embedded gyroscope. When the vehicle-bridge interaction was considered, the fundamental frequency of a bridge was captured using a large set of passing cars with varied speed, stiffness, and mass [22]. The natural frequencies of remote structures in a traffic network were innovatively identified by mounting a smartphone on a moving vehicle by Matarazzo et al. [23].

Quqa et al. [24] installed a smartphone on a stiff and lightweight bicycle to collect the vertical acceleration data of a footbridge. The first mode shape was identified with multiple travels on the bicycle. Multiple mode shapes of the Golden

This work was supported by the Joint Research Centre for Marine Infrastructure. (Corresponding author: Yong Xia.)

Yixian Li, Yuxuan Zhang, and Wanglin Wu are with the Department of Civil and Environmental Engineering, The Hong Kong Polytechnic University, Hong Kong. (e-mail: yixian.li@polyu.edu.hk)

Qi Xia and Tong Guo are with the School of Civil Engineering, Southeast University, Nanjing, China.

Yong Xia is with the Department of Civil and Environmental Engineering and Joint Research Centre for Marine Infrastructure, The Hong Kong Polytechnic University, Hong Kong. ((e-mail: ceyxia@polyu.edu.hk))

Gate Bridge were identified using distributed smartphones [25]. Portable depth sensing on smartphones was used to identify the mode shape in the depth direction [26]. However, only the fundamental mode was accurately identified at a low accuracy in these works because the acceleration data from multiple smartphones are asynchronous and inaccurate. The spectral analysis of asynchronous data is a potential solution [27], and the accuracy of sensors may also be improved by integrating a group of sensors [28].

The smartphone data can even be used to identify structural damage or load information. Mei et al. [29] used the Mel-frequency cepstral coefficients of the vibration data from smartphones to identify damage. Nazar et al. [30] proposed a structural damage detection approach based on the magnetic field intensity variations measured by smartphones. The strain measurement of an SHM system and the smartphone data are fused in a convolutional neural network to classify the speed level and intensity of load in a simply supported bridge experiment [31].

In the mentioned studies, the information between the SHM systems and mobile phones is independent because they are not open to each other. In addition, the SHM data at the local storage centers are unsynchronized with the cloud-based phone data. These facts block the interaction between the infrastructures and phone users (residents, pedestrians, and vehicles). Moreover, the available data are not well fused to generate simple and apparent features for the public because the scientific indexes and criteria cannot be easily used by non-experts. To address these issues, a novel data interaction and fusion framework is developed in this study using heterogeneous data collected via multiple sources. The highlights of this study include the following aspects:

- An infrastructure can interact with its users via heterogeneous data collected by the SHM system and smartphones.
- The temporal, spatial, and spectral effect of users on an infrastructure is modeled and analyzed using the smartphone data collected from the crowd.
- The environmental and structural influence on the uses is quantified by a simple and direct comfort index, where heterogeneous data from the smartphones, SHM system, and online databases are integrated.

The remainder of this paper is organized as follows. The IoT network in urban areas composed of fixed and mobile sensors is introduced in Section II, and it is detailed via an overpassing footbridge in Section III. The bidirectional interactions between the footbridge and pedestrian are investigated in Sections IV to V, followed by discussions and conclusions in Sections VI and VII.

II. IoT Network in a Smart City

A. IoT Network

The facilities and infrastructures nowadays are equipped with sensors to monitor their operational state to achieve a smart city. A huge amount of data is generated in the daily monitoring of structures. Therefore, efficient data fusing and mining algorithms are required to extract valuable information.

In the scenario of bridge SHM shown in Fig. 1, heterogeneous data are collected from various sources, such as the environment, bridge, human, and vehicle traffic. Therefore, the measurement is classified into four categories, namely, environment, pedestrian flow, vehicular traffic, and structural responses, as shown in Fig. 1.

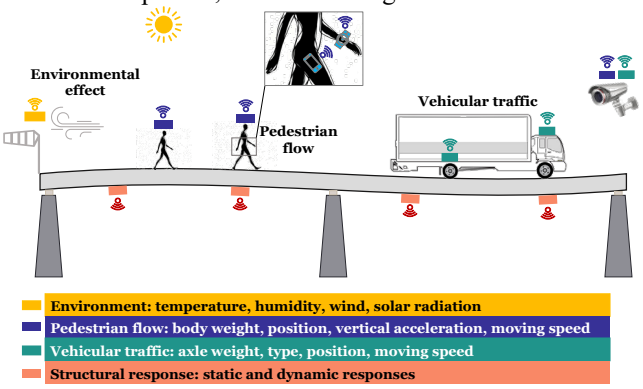

Fig. 1. Schematic of sensor distribution in bridge SHM

The environmental factors include the on-site temperature, humidity, wind speed and direction, and solar radiation, affecting the bridge serviceability and material deterioration. Pedestrian information is collected via wearable facilities, such as smartphones and smartwatches. The pedestrian body weight, position, dynamic acceleration, and moving speed are available with smartphone data accesses. The vehicular information is associated with the vehicle type, axel weight, loading position, and moving speed. The effect of vehicles is more significant than that of pedestrians due to their greater masses. However, the vehicle effect is difficult to monitor because of the unavailability of vehicle data and the gap between vehicle manufacturers and city managers. The structural responses, such as the strain, displacement, acceleration, and settlement, are measured via the SHM system.

Various data are transmitted to and stored at local and online databases via wired and wireless communications, as shown in Fig. 2. The structural response data are usually stored in a local data center, whereas the environmental data are stored in a local meteorological station. Real-time data associated with pedestrians and vehicles are measured via mobile sensors and stored online. The IoT network associated with infrastructure and environment is stationary, whereas that associated with pedestrians and vehicles is mobile and movable.

The interactions between bridge infrastructure, user (pedestrian and vehicle), and environment are also highlighted in Fig. 2. The environmental effects act on the infrastructure and users simultaneously, resulting in the responses of the infrastructure and users. The structural responses include quasi-static deformation and dynamic vibration. Meanwhile, humans can feel comfortable or uncomfortable in the environment, resulting in varying walking and moving

behavior. In addition, the infrastructure and users interact with each other. The structure would deform and vibrate under the action of pedestrians and vehicles, and the users also respond to the over-large structural deformation or vibration.

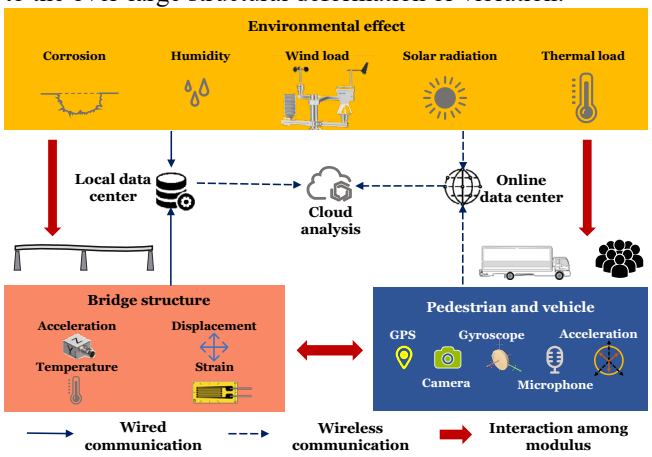

Fig. 2. Data storage, flow, and interaction in an IoT network

The structural responses to environmental effects, such as the thermal and wind loads, are well-studied in existing works and thereby excluded in this study. The environmental effect on users and the interaction between the structure and users are investigated. The schematic of the proposed data interaction framework is presented in Fig. 3. The smartphone-collected data are used to model the dynamic properties of the pedestrian, based on which the structural responses can be reconstructed via finite element (FE) analysis. The SHM system-measured structural accelerations are analyzed to assess the global vibration by using the mode superposition approach. Finally, the data from multiple sources are integrated to evaluate the micro-environment comfort of pedestrians based on a linear comfort model. The proposed approach is expected to outperform existing approaches because the data are collected from the user and infrastructure ends. The analysis results would be more reliable with more information sources.

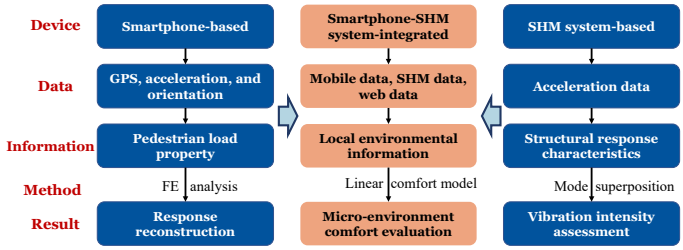

Fig. 3. Schematic of the data interaction framework

B. Mobile Sensing

Nowadays, a smartphone contains different types of micro sensors to monitor its operational states, such as the microphone, accelerometer, gyroscope, camera, compass, and GPS receiver. Smartphone-based mobile sensing becomes a potential complement to conventional SHM due to the huge amount and density of smartphones in modern cities, thereby improving the density and diversity of available data.

In this study, the accelerometer, gyroscope, and GPS receiver in smartphones are used to sense and record the dynamic properties of pedestrians. The accelerometer can measure the accelerations of a pedestrian in three directions, which are decomposed to the global coordinate from the original smartphone coordinate according to the 3D orientations of the smartphone measured by the gyroscope. The GPS data show the positions and traces of the user. When the body weights of smartphone users are known, the static and dynamic components of the pedestrian load can be estimated. The estimated load is consecutively applied to the structural mechanical model to calculate the vibration responses.

The coordinate of a smartphone is displayed in Fig. 4. The right-hand rule is adopted to define the positive direction of rotation. The rotations along the x, y, and z axes are named roll, pitch, and azimuth, respectively. The mapping relationship between the original coordinate (x, y, z) and rotated (x', y', z') is expressed as follows:

$$\begin{bmatrix} x' \\ y' \\ z' \end{bmatrix} = \begin{bmatrix} \cos\beta\cos\gamma & \sin\alpha\sin\beta\cos\gamma - \cos\alpha\sin\gamma & \cos\alpha\sin\beta\cos\gamma + \sin\alpha\sin\gamma \\ \cos\beta\sin\gamma & \sin\alpha\sin\beta\sin\gamma + \cos\alpha\cos\gamma & \cos\alpha\sin\beta\sin\gamma - \sin\alpha\cos\gamma \\ -\sin\beta & \sin\alpha\cos\beta & \cos\alpha\cos\beta \end{bmatrix} \begin{bmatrix} x \\ y \\ z \end{bmatrix} \quad (1)$$

where α, β, and γ denote the rotation degree along x, y, and z axes, respectively. The measured mobile acceleration can be transformed to match the structural coordinate.

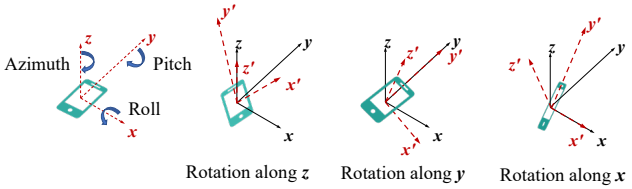

Fig. 4. Coordinate transformation for 3D rotation

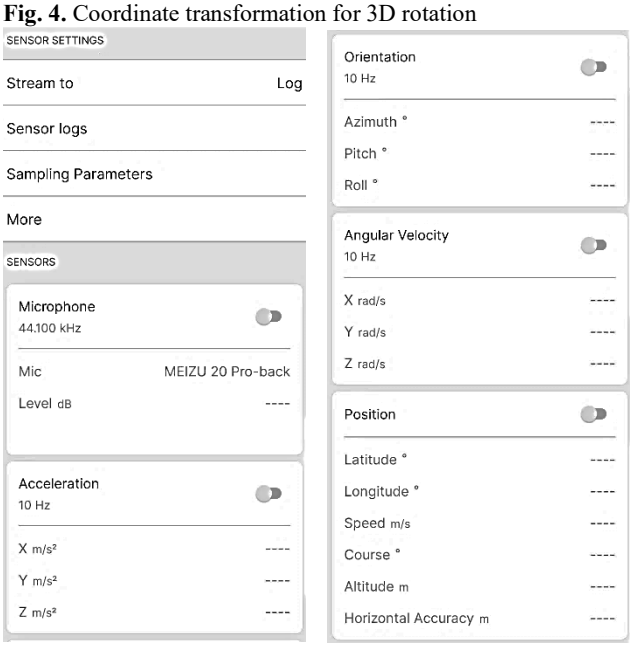

Fig. 5. Interface of sensor log recording

The smartphone sensor record can be accessed and exported by using third-party and open-source applications, such as

MyShake developed by UC Berkeley, *Orion-CC* by Dalian Univ. of Tech., and *MATLAB Mobile* by MathWork Inc. The available applications are well summarized by Sarmadi et al. [32]. *MATLAB Mobile* is adopted in this study due to its stability, flexibility, and cloud transmission function. Its interface is shown in Fig. 5. The sampling rate of sensors can be adjusted between 1 and 100 Hz. The required data can be selected and recorded, and the measurement would finally be transmitted to the cloud for further analysis.

The smartphone-embedded micro sensors are controlled by varied moduli, resulting in inconsistent sampling moments of different data types. Thus, the recorded data should be synchronized for further analysis. A spline function is adopted to interpolate the data time histories and obtain synchronized data. The unsynchronized raw data and synchronized data are shown in Fig. 6 for comparison. Unsynchronized raw data are sampled at varied moments at the given sampling rate, and they are synchronized without distortion by using the spline interpolation approach.

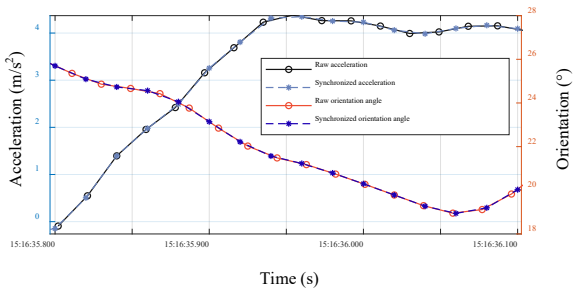

Fig. 6. Resampling sensor records

III. Case Study: A Footbridge

A footbridge shown in Fig. 7 is adopted to study the interaction between infrastructure and users. The footbridge serves as the connection of two buildings on the campus of the Hong Kong Polytechnic University. The bridge is 84.24 m long, consisting of a 64.26 m main span that straddles the highway underneath and a 19.98 m side span. The main steel girder is supported by two steel-tube arches via the steel hangers. One end of the arches is supported on the podium of Block X, and the other end is mounted on the ground of Block Z. The bridge deck is made of concrete.

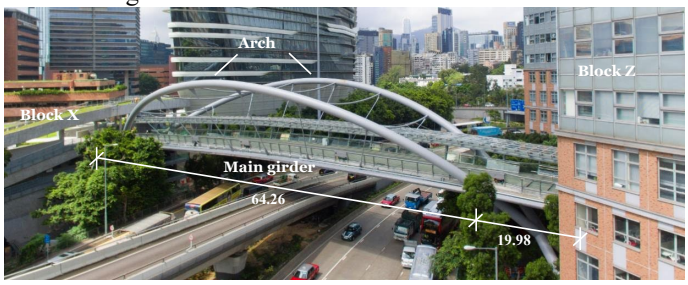

Fig. 7. Overview of the studied footbridge

The FE model of the footbridge was built using the commercial software ANSYS. A beam element model was built to analyze the dynamic structural responses. It is composed of 4939 nodes and 2710 elements. The first six natural frequencies are calculated as 1.80, 2.55, 2.80, 3.56, 3.67, and 5.90 Hz, close to the measured 1.78, 2.60, 2.85, 3.49, 3.61, and 5.91 Hz, verifying the FE model. The first six mode shapes [33] are shown in Fig. 8. The bending and torsional modes of the arch and main girder are coupled due to the special design of the footbridge. The local modes associated with the hangers are neglected.

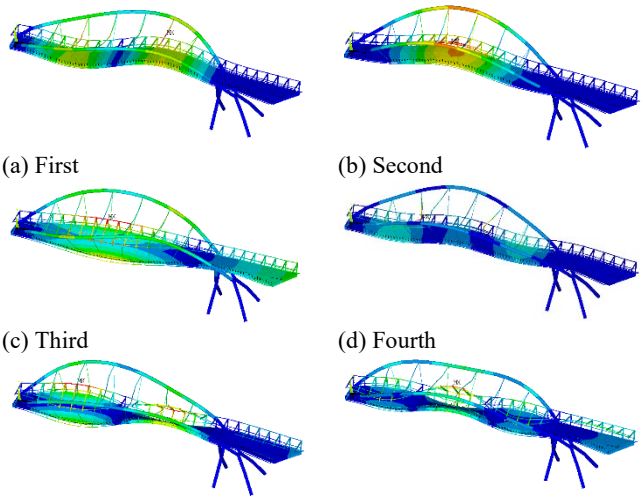

Fig. 8. First six mode shapes

The footbridge is equipped with an SHM system to monitor the environment, pedestrian, and structural responses. The sensor type and corresponding monitoring item are listed in Table 1. The accelerometers, displacement transducers, and strain gauges are used to measure the dynamic and quasi-static structural responses. The closed-circuit cameras, media access control (MAC) sensors, and thermometers measure the pedestrian and thermal loads. Moreover, the weather station, pyranometer, and anemometer are used to monitor the surrounding environment. In this study, the accelerometers are used to investigate the interaction between structure and pedestrian, and the environmental sensors are applied to study the influence of the surrounding environment on the pedestrian. The positions of the sensors used are shown in Fig. 9.

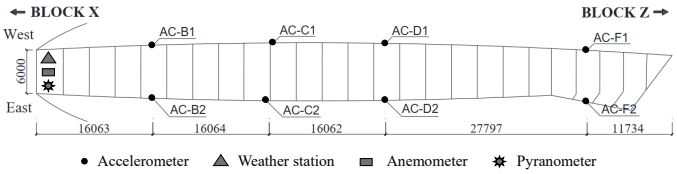

Fig. 9. Positions of the accelerometers and environmental sensors

The environmental effects on the footbridge have already been analyzed in Ref. [34]. In this case study, the interaction between the pedestrians and footbridge is investigated in Sections IV and V.A, and the on-site environmental effects on pedestrians are discussed in Section V.B.

Table 1. List of the installed sensors

Type	Num.	Monitoring parameter	Classification
Accelerometer	8	Acceleration	Dynamic response
Strain gauge	33	Strain	Quasi-static response
Displacement transducer	7	Displacement	Quasi-static and dynamic responses
Thermometer	13	Temperature	Thermal load
Closed-circuit camera	2	Pedestrian location	Pedestrian load
MAC	3	Pedestrian density	Pedestrian load
Weather station	1	Air temperature, humidity, precipitation intensity	Environment
Pyranometer	1	Solar radiation intensity	
Anemometer	1	Wind speed &direction	

IV. Pedestrian Effect on the Footbridge

Pedestrian is the dominant load of a footbridge, especially at a high pedestrian density. Although the SHM system contains close-circuit cameras and MAC sensors to monitor the pedestrian crowd, the human dynamic effect cannot be measured by these sensors. By contrast, mobile facilities can better measure the walking behavior of pedestrians with diverse types of data, and smartphone data are therefore used to analyze the pedestrian effect.

In practice, public smartphone data cannot be accessed. To address this issue, 50 volunteers were asked to walk through the footbridge with a smartphone in their pocket. The smartphone data, including the acceleration, gyroscope, and GPS data, were collected and analyzed. The smartphone-end data are synchronized to standard time since these devices are connected to the internet. The inaccurate data can be detected and removed by using supervised or unsupervised clustering approaches [35], such as the gravitational outlier detector [36]. Moreover, the lost and anomaly data can be recovered from normal data by using the learned mapping relationship among various data [37, 38].

A. Walking Route Analysis using GPS Data

GPS data can be used to identify the position and trace of pedestrians on the footbridge, as shown in Fig. 10. The accuracy of GPS data is related to the available satellites and their positions when the data are recorded. Therefore, some of the recorded points exceed the range of the bridge deck due to the observation uncertainty. In this study, the raw GPS data from mobile phones are directly used without modification.

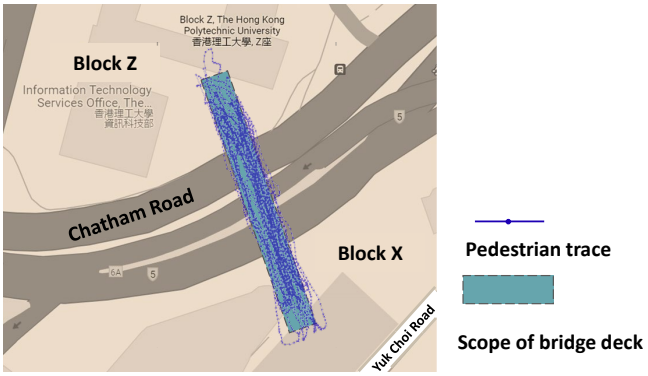

Fig. 10. Recorded pedestrian traces

The GPS data are classified into two categories according to the walking direction inferred from the GPS course data. The north direction is the origin of the course angle. When the monitored course is in a range between 80° and 260°, the associated GPS position data are classified as the category of "ToX," indicating that the pedestrian is traveling from Z block to X block. The remaining data are classified as the "ToZ" category. Subsequently, the *k-means* cluster algorithm is used to collect the latitude and longitude data into 10 clusters, as shown in Fig. 11. The trace centers are nearly identical when pedestrians travel to Blocks X and Z. In reality, pedestrians usually walk on the right side of a lane, which is contradictory to the results in Fig. 11. A possible reason is that the data were collected during traffic-free hours and the pedestrians walked along the center of the footbridge when it was not crowded. These centers are used as the loading position when calculating the pedestrian-induced full-field structural responses.

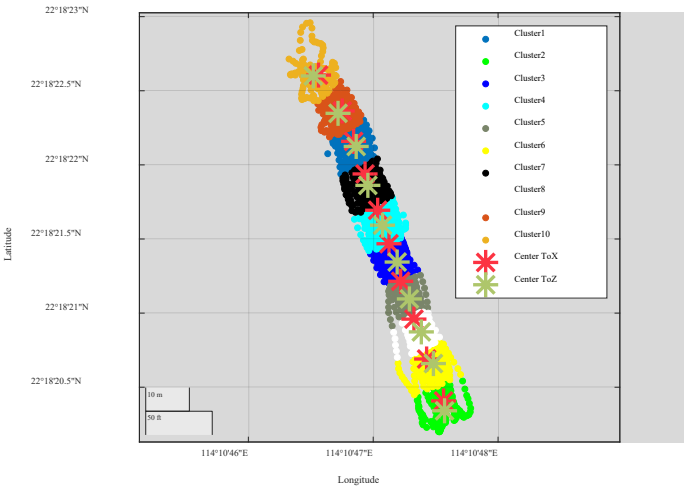

Fig. 11. Clustered latitude and longitude data

B. Modeling Pedestrian Load

The smartphone-embedded accelerometer is used to measure the dynamic effect of pedestrians. Based on the pedestrian moving speed obtained from GPS data, the acceleration records are classified into three categories, namely, slow, medium, and fast walking speeds. The 3D acceleration and orientation data are used to calculate the

vertical acceleration according to Equation (1). The horizontal dynamic load of pedestrians is neglected because it is insignificant compared with the vertical counterpart. Subsequently, the power spectrum densities (PSD) of vertical acceleration are calculated and shown in Fig. 12.

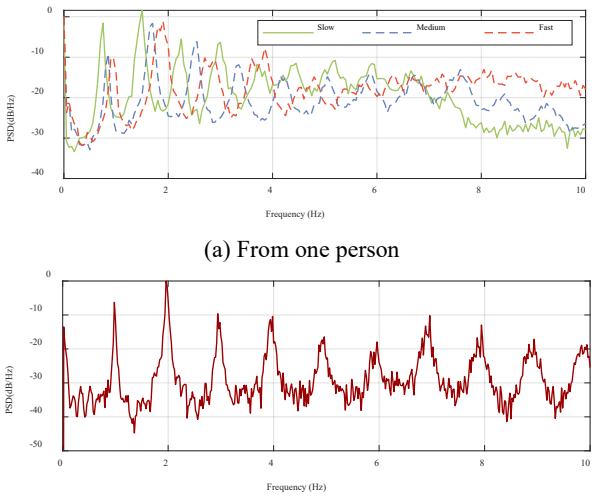

(a) From one person

(b) From crowdsourcing

Fig. 12. PSD of smartphone-embedded accelerations at different walking speeds

The frequency power generated by human steps is lower than 2.1 Hz in most cases, which accords with the PSD distributions in Fig. 12. With the increase in step speed, peaks of the PSD curves shift right, indicating higher step frequency. Moreover, the first two dominant frequencies are 0.75 and 1.50 Hz at slow speed, 0.85 and 1.70 Hz at medium speed, and 0.93 and 1.88 Hz at fast speed in Fig. 12a. The second dominant frequency is approximately two times the first one. This finding is related to the walking pattern of humans: the alternate movement of legs results in the second dominant frequency, and a complete cycle composed of two steps by two legs is associated with the first dominant frequency. The average PSD from all volunteers is calculated and shown in Fig. 12b. It is close to the "Fast" PSD curve in Fig. 12a because all volunteers passed through the footbridge at a fast step rate. This averaged PSD model is used to generate pedestrian load.

The pedestrian load time history is estimated from the averaged PSD S_{f_0} in Fig. 12b using the method proposed by Shinozuka et al. [39]:

$$f(t)=\sqrt{2}\sum_{k=0}^{K}\left(2S_{f_0}(\omega_k)\Delta\omega\right)^{1/2}\cos(\omega_k t+\Phi_k) \qquad (2)$$

where ω_k ($=k\cdot\Delta\omega$) is the discrete frequency with K components, $\Delta\omega$ is the resolution of frequency, and Φ_k is a random number in the range of [0, 2π]. The moving speed of the pedestrians is assumed to be random.

The average body mass of Asians is 57.7 kg, and the standard deviation is reasonably selected as 10 kg [40]. Then, the pedestrian weights (W) can be modeled using a normal distribution. The dynamic load factor (F) is a basic index describing the ratio of the dynamic amplitude of pedestrian load to the human weight. It is experimentally measured by Deng et al. [41] in a range of 0.2 to 0.4. Given the randomly generated body masses and dynamic load factors, the human-induced dynamic load time history can be calculated as follows:

$$p(t)=F\cdot W\cdot\overline{n}(t). \qquad (3)$$

The time history of one of the human-induced loads is shown in Fig. 13. Its PSD is consistent with the targeted PSD in Fig. 12.

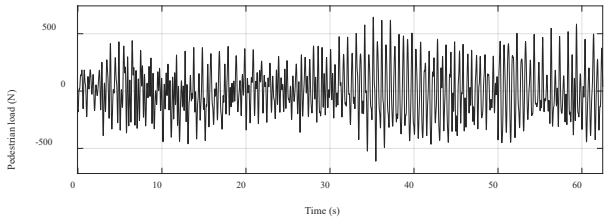

Fig. 13. Artificially generated pedestrian load time history

The artificially generated loads are further applied to the FE model to calculate the structural vibration responses [42]. According to the analysis of Sniady and Sun et al. [43-45], the pedestrian load can be equivalently simplified as the white noise load field that is distributed on the bridge deck. The load lasting for 1 hour is generated and applied to the FE model to calculate the acceleration responses. These loads are applied to the centers of the pedestrian route in Fig. 11.

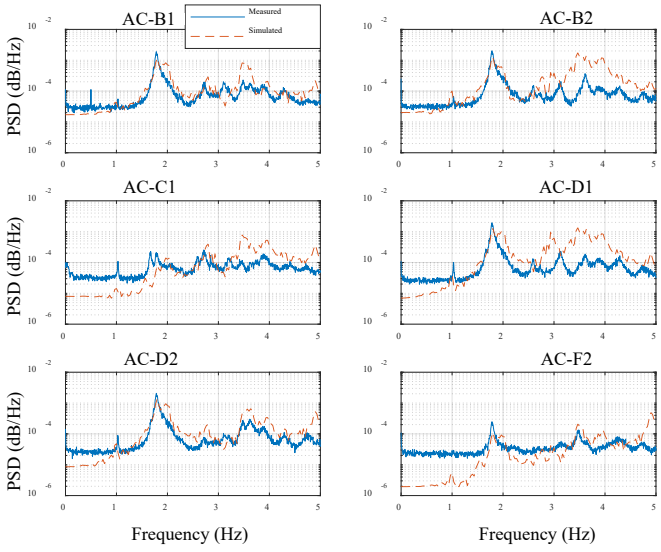

Fig. 14. PSDs of the measured and calculated accelerations on November 3, 2021, from AM 11:00 to AM 12:00

The FE model-calculated accelerations at the sensor positions are extracted. Subsequently, their PSDs are calculated and compared with the measured ones in Fig. 14. The dominant frequencies of different accelerometers vary because the dominant modes at different sensor positions are different. The frequency peak at 1.79 Hz corresponds to the first vertical mode of the footbridge. This peak is the highest for most sensors because the first frequency of the footbridge is close to the step frequency of human walking, as shown in

Fig. 12. The frequency components between 2.50 and 2.85 Hz are associated with the second and third modes. They are insignificant because the frequency power of pedestrians dominates below 2 Hz. Moreover, the frequency power between 3.50 Hz to 3.70 Hz is associated with the fourth and fifth modes. The PSDs above 5 Hz are associated with local modes and randomness of the input load, and they are less accurately reconstructed than the low-frequency ones.

V. Pedestrian Perception of Surroundings

After analyzing the pedestrian effect on the footbridge using the mobile sensor data, the effects of structural vibration and environmental conditions on humans are investigated in this section.

A. Footbridge Vibration

The vibration of a building or bridge causes discomfort to humans. The American [46], European [47], Chinese [48], and ISO [49, 50] codes limit the structural maximum acceleration in operation. Feng et al. [51] tested the vibration comfort of several footbridges in Beijing using the maximum acceleration measured by a uniaxial accelerometer. In existing field testing and design codes, the acceleration response at a moveless position is used to evaluate the comfort level of vibration. By contrast, the vibration comfort of the present footbridge is comprehensively evaluated using the distributed accelerometers and FE model. The acceleration data are synchronized by using the timestamp of the SHM system. The timestamp of the SHM system is consistent with those of smartphones as the data acquisition system of modern SHM systems uses a GPS timer, which is adequately accurate for SHM applications.

The vibration dose value (VDV) is adopted as the indicator to measure the intensity of vibration in a period. VDV is calculated as follows:

$$VDV = \frac{1}{T}\int_0^T a(t)^4 dt, \tag{4}$$

where T is the length of time, and $a(t)$ is the acceleration time history; here, T is 1 minute. VDVs are calculated using the recorded acceleration data on November 3–10, 2021, as shown in Fig. 15. The VDVs periodically fluctuated in the study duration of eight days. VDVs increased during the daytime and decreased at night because pedestrians were rare at night. Moreover, the VDVs calculated from accelerometers at different locations differ substantially from each other. The VDVs at C1, C2, F1, and F2 are remarkably less than those of B1, B2, D1, and D2 because the latter four accelerometers are near the peak and valley of the first mode shape, as shown in Fig. 8 and Fig. 9. The first mode response dominates the dynamic vibration of the footbridge in most of the operation time. Therefore, the VDVs of B1, B2, D1, and D2 are more significant than the others.

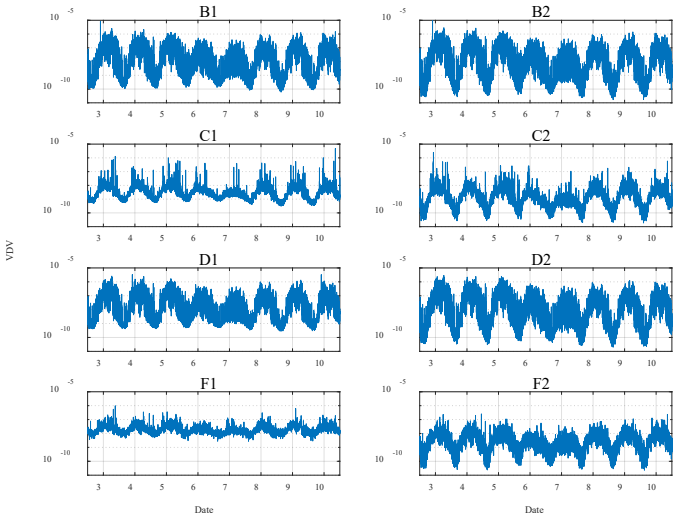

Fig. 15. VDVs of different accelerometers during eight days

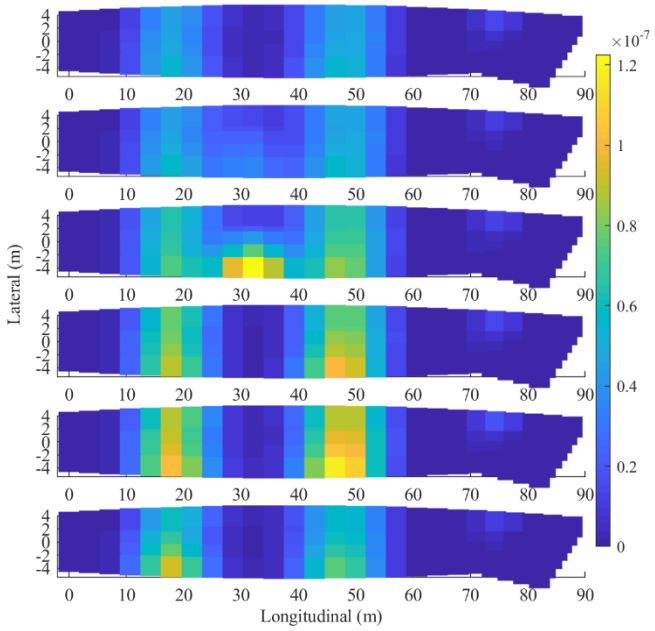

Fig. 16. VDV on the bridge deck in one hour

The VDV on the entire bridge deck can be further estimated by integrating the acceleration data and FE model-calculated mode shapes. The vertical accelerations on the whole bridge deck are calculated by using the mode superposition technique, in which eight accelerometers and the first six modes are used. The VDVs on the bridge deck from 11:00 to 12:00 on November 3, 2021 are calculated, and the averaged VDVs in 10 minutes are displayed in Fig. 16. Then, the spatiotemporal characteristics of VDVs can be investigated. The VDVs in the last 40 minutes are higher than those in the first 20 minutes, which is easily determined from the magnitudes of the VDVs. In addition, the dominant modes are different in varied periods. The first mode, a bending mode, dominates the vibration from 11:00 to 11:10. The third mode, a torsional mode, dominates the vibration from 11:20 to 11:30, and the VDV in this period is the highest in the studied one

hour. In the remaining periods, the vibration is the combination of the bending and torsional modes. The expanded VDV on the entire bridge deck can evaluate the serviceability of the footbridge more comprehensively than the conventional indexes confined to the sensor positions.

B. Micro-environment

The perception of humans is highly related to the micro-environment. In meteorological monitoring, the spatial resolution of data is insufficient to obtain the required information about the micro-environment. The SHM system, which includes a micro weather monitoring station, can compensate for this issue.

Human comfort is determined by several factors, including air temperature, humidity, solar radiation intensity, surrounding wind speed, air quality, and noise level. In this study, the linear comfort evaluation model developed by Ma et al. [52] is adopted to calculate the comfort index of pedestrians, as shown in Fig. 17. This model was established via a questionnaire survey in Hong Kong and regression analysis. It applies to the seasons from autumn to spring when the temperature is not very high. Human comfort and environmental factors, such as temperature, are not linearly dependent, which is unconsidered in the linear comfort model. This limitation should be improved using a more sophisticated comfort evaluation model in the future.

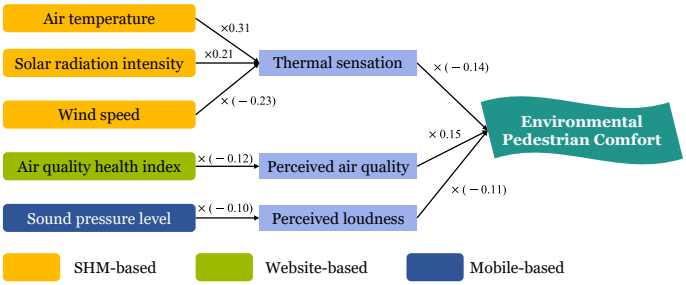

Fig. 17. Linear comfort evaluation model of micro-environment

Three types of data are included in Fig. 17, namely, SHM, Web, and mobile data. The air temperature, solar radiation intensity, and wind speed data are extracted from the SHM system. The air quality data are downloaded from the website of the air quality health index of Hong Kong at https://www.aqhi.gov.hk. The noise level can be directly measured by a smartphone-embedded microphone. After obtaining online and offline data, heterogeneous data are normalized using the normalization factors provided in Ref. [52]. Subsequently, the pedestrian comfort indexes on November 3–10, 2021 are calculated and shown in Fig. 18.

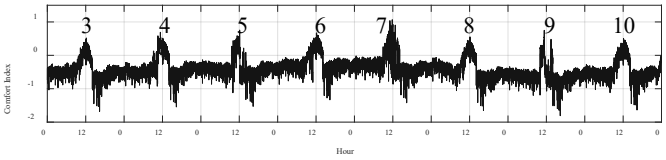

(a) Solar radiation data are included

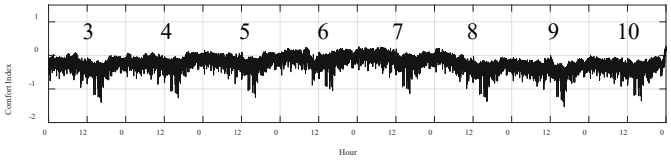

(b) Solar radiation data are excluded

Fig. 18. Comfort index from November 3 to 10, 2021

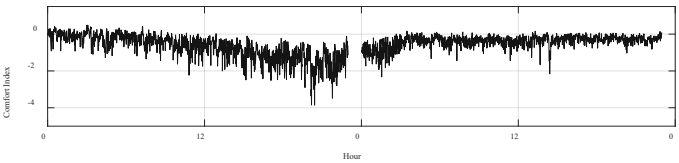

Fig. 19. Comfort index from September 1 to 2, 2023 in the typhoon weather

In Fig. 18a, the comfort index during the daytime is much higher than that after sunset, indicating that the contribution of solar radiation is significant. The original comfort evaluation model is established for urban streets, where the light intensity is an essential factor. Considering that the footbridge is equipped with a lighting system, the comfort of pedestrians is not highly influenced by the natural light intensity. Therefore, the factor of solar radiation is eliminated from the comfort model, and the comfort index is calculated and shown in Fig. 18b. The calculated comfort index fluctuates periodically. The comfort index in the afternoons is lower than that of the remaining time in one day because the air quality in the afternoon is the poorest, and meanwhile, the wind speed is higher. Moreover, the overall comfort index decreased slightly after Nov. 8 as a result of the reduction in air temperature.

Moreover, the comfort index is calculated in the extreme typhoon weather with the contribution of solar radiation being eliminated. The monitored data from September 1 to 2, 2023 are used when typhoon Kirogi was approaching Hong Kong. The recorded maximum wind speed was 27.25 m/s. The calculated comfort index is shown in Fig. 9, which is less than that in Fig. 18b because the wind speed is negatively related to the comfort level. The minimum comfort index appears at the moment when the wind speed is maximum. These results demonstrate that the proposed framework applies to the extreme conditions as well.

The comfort of pedestrians is evaluated in this section by considering the vibration intensity and micro-environment. In extreme conditions, such as poor weather or severe vibration of the bridge, the comfort indexes could be reduced significantly, providing serviceability information for the managers. The heterogeneous data-based comfort evaluation framework can improve the intelligence and serviceability of the footbridge.

VI. Prospect

The heterogeneous data interaction framework is applied to a footbridge to exemplify how it works. It can be further used for city-scale data management with access to the public data and sufficient computing resources. The infrastructures

equipped with the SHM systems can be modeled, analyzed, and integrated with the associated crowd-sourced smartphone data.

Modeling the infrastructures is the most laborious work because the configurations of civil structures are diverse, and the associated cost is proportional to the number and size of the infrastructures. In contrast, the computational cost in data analysis is much lower. The computational time is 9 min 4 s in Section V.A, where eight days of data are included, with the computer configuration of Intel (R) Core (TM) i7-10875H CPU @ 2.30GHz. The cost of smartphone data mining is proportional to the length of data × number of smartphones. The overall data processing time in Section IV is 0.46 s associating with 50 participants. Moreover, the environmental comfort index is estimated by linear operators, and the associated computational time in Section V.B is 0.003 s. Therefore, the proposed framework is generally scalable with more participants. However, the FE models of all infrastructures should be established when the framework is scaled to urban-scale application, and this process requires much more resources and time than the data interaction algorithms themselves.

VII. Conclusions

The IoT sensing network in modern city is utilized to link the infrastructures and users, realizing bidirectional interaction of information from multiple sources. The data accessed from the SHM system, mobile smartphones, and online database are fused and interact with each other to improve the intelligence of infrastructures. A footbridge is used as a testbed.

Heterogeneous and unsynchronized data are recorded by the sensors embedded in smartphones. The GPS data are used to analyze the traces of pedestrians, and the acceleration data are adopted to estimate the power spectrum density of human load. Then, a human load field is generalized using the pedestrian information dataset, and it is applied to the mechanical model of the footbridge to calculate the bridge dynamic responses, which are consistent with the measurement. At the same time, the environmental and vibration data, accessed through the SHM system and online database, are used to evaluate the users' perception via two comfort indexes, namely, the vibration dose value and walking conform index to micro-environment. These indexes fluctuate with the variation of environment and pedestrian traffic in one day. In the closed data cycle, the infrastructure and user ends can share, fuse, and integrate heterogeneous information to accomplish the interaction among human beings and urban facilities.

Acknowledgment

The authors sincerely appreciate the financial support received from the Joint Research Centre for Marine Infrastructure.

References

[1] R. Du *et al.*, "The Sensable City: A Survey on the Deployment and Management for Smart City Monitoring," *Ieee Communications Surveys and Tutorials,* vol. 21, no. 2, pp. 1533-1560, 2019, 2019.

[2] Q. Meng, P. Lu, and S. Zhu, "A Smartphone-Enabled IoT System for Vibration and Noise Monitoring of Rail Transit," *Ieee Internet of Things Journal,* vol. 10, no. 10, pp. 8907-8917, May 15, 2023.

[3] L. M. Sun *et al.*, "Hybrid monitoring methodology: A model-data integrated digital twin framework for structural health monitoring and full-field virtual sensing," *Advanced Engineering Informatics,* vol. 60, Apr, 2024.

[4] J. P. Feng *et al.*, "A deep learning-based interferometric synthetic aperture radar framework for abnormal displacement deformation prediction of bridges," *Advances in Structural Engineering,* vol. 26, no. 16, pp. 3005-3020, Dec, 2023.

[5] Y. Zhu, and H. Tang, "Automatic Damage Detection and Diagnosis for Hydraulic Structures Using Drones and Artificial Intelligence Techniques," *Remote Sensing,* vol. 15, no. 3, Feb, 2023.

[6] L. Sun *et al.*, "Review of Bridge Structural Health Monitoring Aided by Big Data and Artificial Intelligence: From Condition Assessment to Damage Detection," *Journal of Structural Engineering,* vol. 146, no. 5, May, 2020.

[7] R. K. Verma *et al.*, "Damage detection in bridge structures: An edge computing approach," *arXiv preprint arXiv:2008.06724*, 2020.

[8] Y. Bao, and H. Li, "Machine learning paradigm for structural health monitoring," *Structural Health Monitoring-an International Journal,* vol. 20, no. 4, pp. 1353-1372, Jul, 2021.

[9] L. S. Lanxin Luo, Yixian Li, and Yong Xia, "Structural Nonlinear Boundary Condition Identification Using A Hybrid Physics Data-driven Approach," *Nonlinear Dynamics*, 2025.

[10] Q. Xia *et al.*, "System design and demonstration of performance monitoring of a butterfly-shaped arch footbridge," *Structural Control & Health Monitoring,* vol. 28, no. 7, Jul, 2021.

[11] L. F. Li *et al.*, "Thermal behaviors of bridges - A literature review," *Advances in Structural Engineering,* vol. 26, no. 6, pp. 985-1010, Apr, 2023.

[12] Z. Lai *et al.*, "Neural modal ordinary differential equations: Integrating physics-based modeling with neural ordinary differential equations for modeling high-dimensional monitored structures," *Data-Centric Engineering,* vol. 3, 2022, 2022.

[13] Y. X. Li *et al.*, "Principal force pattern and impulse response mode for structural equivalent force estimation and full-field response reconstruction," *Mechanical Systems and Signal Processing,* vol. 200, Oct, 2023.

[14] X. Jian, Y. Xia, and L. Sun, "An indirect method for bridge mode shapes identification based on wavelet analysis," *Structural Control & Health Monitoring,* vol. 27, no. 12, Dec, 2020.

[15] X. Jian, Y. Xia, and L. Sun, "Indirect identification of bridge frequencies using a four-wheel vehicle: Theory and three-dimensional simulation," *Mechanical Systems and Signal Processing,* vol. 177, Sep 1, 2022.

[16] A. Capponi *et al.*, "A Survey on Mobile Crowdsensing Systems: Challenges, Solutions, and Opportunities," *Ieee Communications Surveys and Tutorials,* vol. 21, no. 3, pp. 2419-2465, 2019.

[17] H. Sarmadi *et al.*, "Review on smartphone sensing technology for structural health monitoring," *Measurement,* vol. 223, Dec, 2023.

[18] D. Y. Zhang, J. D. Tian, and H. Li, "Design and Validation of Android Smartphone Based Wireless Structural Vibration Monitoring System," *Sensors,* vol. 20, no. 17, Sep, 2020.
[19] A. B. Noel *et al.*, "Structural Health Monitoring Using Wireless Sensor Networks: A Comprehensive Survey," *Ieee Communications Surveys and Tutorials,* vol. 19, no. 3, pp. 1403-1423, 2017.
[20] M. Feng *et al.*, "Citizen Sensors for SHM: Use of Accelerometer Data from Smartphones," *Sensors,* vol. 15, no. 2, pp. 2980-2998, Feb, 2015.
[21] E. Ozer, and M. Q. Feng, "Direction-sensitive smart monitoring of structures using heterogeneous smartphone sensor data and coordinate system transformation," *Smart Materials and Structures,* vol. 26, no. 4, Apr, 2017.
[22] N. Shirzad-Ghaleroudkhani, Q. Mei, and M. Gul, "Frequency Identification of Bridges Using Smartphones on Vehicles with Variable Features," *Journal of Bridge Engineering,* vol. 25, no. 7, Jul 1, 2020.
[23] T. J. Matarazzo *et al.*, "Crowdsensing Framework for Monitoring Bridge Vibrations Using Moving Smartphones," *Proceedings of the Ieee,* vol. 106, no. 4, pp. 577-593, Apr, 2018.
[24] S. Quqa, P. F. Giordano, and M. P. Limongelli, "Shared micromobility-driven modal identification of urban bridges," *Automation in Construction,* vol. 134, Feb, 2022.
[25] E. Ozer, R. Purasinghe, and M. Q. Feng, "Multi-output modal identification of landmark suspension bridges with distributed smartphone data: Golden Gate Bridge," *Structural Control & Health Monitoring,* vol. 27, no. 10, Oct, 2020.
[26] G. R. Tondo, C. Riley, and G. Morgenthal, "Characterization of the iPhone LiDAR-Based Sensing System for Vibration Measurement and Modal Analysis," *Sensors,* vol. 23, no. 18, Sep, 2023.
[27] Y. C. Zhu, and S. K. Au, "Spectral characteristics of asynchronous data in operational modal analysis," *Structural Control & Health Monitoring,* vol. 24, no. 11, Nov, 2017.
[28] H. Jo *et al.*, "Feasibility of displacement monitoring using low-cost GPS receivers," *Structural Control & Health Monitoring,* vol. 20, no. 9, pp. 1240-1254, Sep, 2013.
[29] Q. P. Mei, and M. Gul, "A crowdsourcing-based methodology using smartphones for bridge health monitoring," *Structural Health Monitoring-an International Journal,* vol. 18, no. 5-6, pp. 1602-1619, Nov, 2019.
[30] A. M. Nazar *et al.*, "A New Structural Health Monitoring Approach Based on Smartphone Measurements of Magnetic Field Intensity," *Ieee Instrumentation & Measurement Magazine,* vol. 24, no. 4, pp. 49-58, Jun, 2021.
[31] S. Mustapha *et al.*, "Estimation of crowd flow and load on pedestrian bridges using machine learning with sensor fusion," *Automation in Construction,* vol. 112, Apr, 2020.
[32] H. Sarmadi *et al.*, "Review on smartphone sensing technology for structural health monitoring," *Measurement,* vol. 223, Dec, 2023.
[33] B. Szabó, and I. Babuška, "Finite element analysis: Method, verification and validation," 2021.
[34] Q. Xia *et al.*, "Temperature behaviors of an arch bridge through integration of field monitoring and unified numerical simulation," *Advances in Structural Engineering,* vol. 25, no. 16, pp. 3492-3509, Dec, 2022.
[35] Y. Q. Bao *et al.*, "Computer vision and deep learning-based data anomaly detection method for structural health monitoring," *Structural Health Monitoring-an International Journal,* vol. 18, no. 2, pp. 401-421, Mar, 2019.
[36] S. Bharti, and K. K. Pattanaik, "Gravitational outlier detection for wireless sensor networks," *International Journal of Communication Systems,* vol. 29, no. 13, pp. 2015-2027, Sep, 2016.
[37] G. Fan, J. Li, and H. Hao, "Lost data recovery for structural health monitoring based on convolutional neural networks," *Structural Control & Health Monitoring,* vol. 26, no. 10, Oct, 2019.
[38] Y. X. Li *et al.*, "Finite element model-informed deep learning for equivalent force estimation and full-field response calculation," *Mechanical Systems and Signal Processing,* vol. 206, Jan, 2024.
[39] M. Shinozuka, and G. Deodatis, "Simulation of stochastic processes by spectral representation," 1991.
[40] S. C. Walpole *et al.*, "The weight of nations: an estimation of adult human biomass," *BMC public health,* vol. 12, no. 1, pp. 1-6, 2012.
[41] D. Y. Deng *et al.*, "Experimental Investigation on Pedestrian Walking Load in Steel Footbridges," *Frontiers in Materials,* vol. 9, Jun, 2022.
[42] R. Clough, and J. Penzien, *Dynamics of Structures*: McGraw-Hill NY, USA, 1975.
[43] P. Śniady, "Vibration of a beam due to a random stream of moving forces with random velocity," *Journal of Sound and Vibration,* vol. 97, no. 1, pp. 23-33, 1984.
[44] L. Sun, and X. Deng, "Predicting vertical dynamic loads caused by vehicle-pavement interaction," *Journal of transportation engineering,* vol. 124, no. 5, pp. 470-478, 1998.
[45] T. Golecki *et al.*, "Continuous random field representation of stochastic moving loads," *Probabilistic Engineering Mechanics,* vol. 68, Apr, 2022.
[46] AASHTO, "Guide specifications for design of FRP pedestrian bridges," AASHTO, 2008.
[47] C. E. C. f. Standardization), "Design of concrete structures," *Part 2: Concrete bridge*, 1996.
[48] B. M. E. R. Institute, ". Technical specifications of urban pedestrian overcrossing and underpass," 1996.
[49] ISO, "Mechanical vibration and shock: Evaluation of human exposure to whole-body vibration," *Part 1: General requirements*, ISO, 1997.
[50] ISO, "Bases for design of structures: Serviceability of buildings and walkways against vibrations," ISO, 2007.
[51] P. Feng *et al.*, "Vibration Serviceability Assessment of Pedestrian Bridges Based on Comfort Level," *Journal of Performance of Constructed Facilities,* vol. 33, no. 5, Oct 1, 2019.
[52] X. Ma, C. K. Chau, and J. H. K. Lai, "Critical factors influencing the comfort evaluation for recreational walking in urban street environments," *Cities,* vol. 116, Sep, 2021.